EHD2 overexpression promotes tumorigenesis and metastasis in triple-negative breast cancer by regulating store-operated calcium entry

Haitao Luan[1,*], Timothy A. Bielecki[1,*], Bhopal C. Mohapatra[2,*,8], Namista Islam[1,2], Insha Mushtaq[1,3], Aaqib M. Bhat[1,2], Sameer Mirza[2], Sukanya Chakraborty[1,2], Mohsin Raza[2], Matthew D. Storck[1], Jane L. Meza[4,8], Wallace B. Thoreson[5], Donald W. Coulter[6,8], Emad A. Rakha[7], Vimla Band[2,8,#], Hamid Band[1,2,3,8,#]

[1]Eppley Institute for Research in Cancer and Allied Diseases, University of Nebraska Medical Center, NE 68198, USA; [2]Departments of Genetics, Cell Biology & Anatomy, College of Medicine, University of Nebraska Medical Center, NE 68198, USA; [3]Departments of Pathology & Microbiology, College of Medicine, University of Nebraska Medical Center, NE 68198, USA; [4]Departments of Biostatistics, College of Public Health, University of Nebraska Medical Center, NE 68198, USA; [5] Stanley M. Truhlsen Eye Institute, University of Nebraska Medical Center, NE 68198, USA; [6]Department of Pediatrics, University of Nebraska Medical Center, NE 68198, USA; [7]Department of Histopathology, Nottingham University Hospital NHS Trust, City Hospital Campus, Nottingham, NG5 1PB, UK; [8]Fred & Pamela Buffett Cancer Center, University of Nebraska Medical Center, NE 68198, USA.

Current Address: TAB, Sanofi US, Cambridge, MA 02142

*Co-First Authors

Running Title: EHD2-SOCE axis in TNBC tumorigenesis

Financial Supports: This research was funded by: the Department of Defense grants W81XWH-17-1-0616 and W81XWH-20-1-0058 to HB and W81XWH-20-1-0546 to VB; the NIH grants R21CA241055 and R03CA253193 to VB; pilot grants from the Fred & Pamela Buffett Cancer Center (HB & VB); the Raphael Bonita Memorial Fund; and support to UNMC core facilities from the NCI Cancer Center Support Grant (P30CA036727) awarded to Fred & Pamela Buffett Cancer Center and from the Nebraska Research Initiative. TAB, AMB and SC received University of Nebraska Medical Center Graduate Student Fellowships.

#**Corresponding authors:** Hamid Band, MD, PhD, Eppley Institute for Research in Cancer and Allied Disease, 986805 Nebraska Medical Center, Omaha, NE 68198-6805, USA; Email: hband@unmc.edu; Phone: 402-559-8572

Vimla Band, PhD, Department of Genetics Cell Biology & Anatomy, University of Nebraska Medical Center, 985805 Nebraska Medical Center, Omaha, NE, 68198, USA. vband@unmc.edu; Phone: 402-559-8565

Conflict of interest disclosure statement: Dr. H. Band and Dr. V. Band received funding from Nimbus Therapeutics for an unrelated project.

Word count: Abstract-144, Manuscript-5037

Figures: 8; **Supplementary**: 7 Figures and 1 table

Abstract:

With nearly all cancer deaths a result of metastasis, elucidating novel pro-metastatic cellular adaptations could provide new therapeutic targets. Here, we show that overexpression of the EPS15-Homology Domain-containing 2 (EHD2) protein in a large subset of BCs, especially the triple-negative (TNBC) and HER2+ subtypes, correlates with shorter patient survival. The mRNAs for EHD2 and Caveolin-1/2, structural components of caveolae, show co-overexpression across breast tumors, predicting shorter survival in basal-like BC. ShRNA knockdown and CRISPR-Cas9 knockout of EHD2, together with mouse EHD2 rescue, in TNBC cell line models demonstrate a major positive role of EHD2 in promoting tumorigenesis and metastasis. Mechanistically, we link these roles of EHD2 to store-operated calcium entry (SOCE), with EHD2-dependent stabilization of plasma membrane caveolae ensuring high cell surface expression of the SOCE-linked calcium channel Orai1. The novel EHD2-SOCE oncogenic axis represents a potential therapeutic target in EHD2 and CAV1/2-overexpressing BC.

Introduction:

Breast cancer (BC) remains a major cause of cancer-related deaths, with less than 30% 5-year survival rate in patients with metastatic disease (www.acs.org). Triple-negative BC (TNBC) presents a particularly difficult diagnosis with lack of targeted therapies. A better understanding of tumorigenesis- and metastasis-associated cellular adaptations could open new approaches to improve the survival of TNBC patients.

EPS15-homology (EH) domain-containing (EHD) proteins (EHD1-4) are evolutionarily-conserved lipid membrane-activated ATPases that regulate inward or outward vesicular traffic between plasma membrane and intracellular organelles by controlling tubulation and scission of trafficking vesicles (1). Unlike other family members, which predominantly localize to endosomal and other intracellular compartments, EHD2 primarily localizes to plasma membrane caveolae to maintain their stable membrane pool (2, 3), suggesting a likely role in caveolae-associated cellular functions. Indeed, caveolae-dependent fatty acid uptake in adipocytes and e-NOS-NO induced small blood vessel relaxation are impaired in EHD2 knockout mice (4, 5). EHD2 stabilization of caveolae was also found to promote the cell surface expression of ATP-sensitive K^+ channels and protect cardiomyocytes against ischemic injury (6). Caveolae are key to buffering the plasma membrane stress (7) and EHD2 has been shown to positively regulate mechano-transduction by regulating transcriptional programs (8). Recent studies have painted a complex picture of the potential roles of EHD2 in cancer. Reduced EHD2 expression was reported in esophageal, colorectal, , breast, and hepatocellular cancers(9-12), with in vitro knockdown or overexpression studies supporting a tumor suppressive role for EHD2. On the contrary, EHD2 overexpression was found as a component of a mesenchymal signature in malignant gliomas with shorter survival, and knockdown analyses showed EHD2 requirement

for cell proliferation, migration and invasion (13). Higher EHD2 mRNA expression in papillary thyroid carcinomas was associated with extrathyroidal extension, lymph node metastasis, higher risk of recurrence, and presence of BRAF-V600E mutation (14). Studies of clear cell renal cell carcinoma also supported a positive role of EHD2 in tumorigenesis (15). A recent study provided a more mixed picture, with loss of EHD2 expression in TNBC cell lines enhancing their proliferation, migration, and invasion but low levels of EHD2 mRNA in TNBC patient tumors predicting better prognosis (16). Thus, a definitive role of EHD2 in oncogenesis and its mechanisms remain unclear.

Here, our comprehensive expression analyses in BC samples and in vitro and in vivo studies using EHD2 knockdown or knockout approaches in TNBC cell models provide definitive evidence for strong pro-tumorigenic and pro-metastatic role of EHD2 through a novel mechanism, namely its requirement for efficient store-operated calcium entry (SOCE), a pathway known to promote tumorigenesis and metastasis in breast and other cancers (17, 18).

Results:

EHD2 is expressed in basal cells of the mouse mammary gland and in a subset of basal-like breast cancer cell lines

First, we used immunoblotting and immunofluorescence staining of mammary gland tissue from control and *Ehd2*-null mice (generated in the lab; unpublished) to authenticate the specific recognition of EHD2 by an antibody previously validated against ectopic tagged-EHD2 (19) (**Supplementary Fig. S1A-B**). High EHD2 expression was seen in mammary adipocytes, consistent with high EHD2 expression in adipose tissues (20). Moderate/high EHD2 staining was seen in the mammary basal/myoepithelium (smooth muscle actin^{+}), but little in the luminal

epithelium (cytokeratin 8^{+}) (**Supplementary Fig. S1C**). The basal/myoepithelial cell selective localization was confirmed by immunohistochemistry (IHC) (**Supplementary Fig. S1D**). Immunoblotting of basal (EPCAM-low/CD29-high) and luminal (EPCAM-high/CD29-low) mouse mammary epithelial organoids further confirmed the basal cell expression of EHD2 (**Supplementary Fig. S1E**). Thus, while mammary adipocytes express the highest EHD2, within the epithelium the basal epithelial cells show selective EHD2 expression.

By immunoblotting, we found EHD2 expression in immortal basal-like mammary epithelial cell lines 76Ntert (hTert-immortalized primary mammary epithelial cell line) (21) and MCF10A, in 2 out of 3 TNBC cell lines, and at lower levels in 3 out of 11 HER2+ cell lines, but in none of the 9 luminal A/B BC cell lines (**Supplementary Fig. S2A**). Notably, our cell line results were discordant with reports of comparable EHD2 expression in MCF-7 (luminal), MDA-MB415 (luminal) and MDA-MB-231 (basal) cell lines (11, 22). Immunofluorescence analysis of selected cell lines confirmed the expression pattern seen in immunoblotting and showed exclusive localization of EHD2 to the plasma membrane and cytoplasm (**Supplementary Fig. S2B**). Thus, EHD2 expression is a feature of normal basal mammary epithelial cells and a subset of the basal-like BC.

EHD2 overexpression is associated with metastasis and shorter survival in breast cancer

Based on the above findings, we conducted IHC staining a tissue microarray (TMA) with 840 primary BC samples from a well-annotated patient cohort (23)to assess the expression of EHD2. Given the cytoplasmic/membrane localization of EHD2 in the mammary gland and BC cell lines, we quantified IHC signals as cytoplasmic and nuclear (**Fig. 1A**). 759 and 756 cases respectively showed a valid positive/negative cytoplasmic or nuclear signal (**Supplementary**

Table 1A). High cytoplasmic and low nuclear EHD2 signals showed a positive association with higher tumor grade, higher mitosis, and lower cyokeratin-5 expression while high nuclear EHD2 signals showed a reverse correlation and was associated with ER/PR/AR-positive and non-TNBC status (**Supplementary Table 1B**). High cytoplasmic EHD2 predicted shorter BC-specific survival, while high nuclear EHD2 showed an opposite correlation (**Fig. 1B**). Across BC subtypes, the high cytoplasmic and nuclear-negative EHD2, which also predicted shorter BC-specific survival (**Supplementary Fig. S2C**), was seen in about half of TNBC and HER2+ samples, and a third of ER+ samples (**Fig. 1C, Supplementary Table 1B**). Thus, our results indicate that high cytoplasmic EHD2 expression, a localization similar to that observed in normal mammary epithelium and BC cell lines, is a marker of more aggressive BC, contrary to published reports that did not report assess cytoplasmic/nuclear EHD2 and suggested its potential tumor suppressor role (11, 16, 22).

EHD2 knockdown or knockout in TNBC cell lines impairs the tumorigenic and pro-metastatic traits

To examine the role of EHD2 expression in BC oncogenesis, we established control or EHD2 shRNA expressing TNBC cell lines, Hs578T, BT549 and MDA-MB-231 (**Fig. 2A**). While EHD2 knockdown (KD) did not affect proliferation in two-dimensional culture on plastic (**Fig. 2B**), it markedly reduced the tumorsphere growth under low attachment (**Fig. 2C**), impaired invasion across Matrigel in trans-well assays (**Fig. 2D**) and markedly reduced the invasive fronts in a Matrigel organoid invasion assay (**Fig. 2E**).

Orthotopically implanted control Hs578T cells expected produced xenograft tumors over time while EHD2 KD cells showed a severe reduction in tumor formation (**Fig. 2F**). Immuno-

staining confirmed the EHD2 KD (**Fig. 2G**) and showed marked reduction in proliferation ($Ki67^{+}$) with sparse tumor cells in H&E sections (**Fig. 2H**). EHD2 KD in MDA-MB-231 cells also reduced the xenograft growth and frequency of lung tumor metastasis (**Supplementary Fig. S3**).

Further, CRISPR-Cas9-mediated EHD2 knockout (KO) in TNBC cell lines (**Fig. 3A**) significantly impaired their cell migration, invasion (**Fig. 3B-C, Supplementary Fig. S4A-B**) and extracellular matrix (ECM) degradation (**Fig. 3D, supplementary Fig. S4C**), another pro-metastatic trait (24). Introduction of mouse EHD2 in MDA-MB-231 EHD2-KO cells, at levels lower than in control cells, significantly rescued the cell migration defect (**Fig. 3E**), demonstrating specificity. Reciprocally, CRISPR activation of endogenous EHD2 in EHD2-nonexpressing MDA-MB-468 TNBC cells (**Fig. 3F)** increased cell migration compared to control cells (**Fig. 3G**). When orthotopically implanted in nude mice, EHD2 KO MDA-MB-231 cells exhibited a marked and significant defect in tumor formation, with a significant rescue upon mouse EHD2 expression (**Fig. 3H**).

To directly assess the role of EHD2 in metastasis, luciferase-expressing control and KO MDA-MB-231 cells were intravenously injected into nude mice. Luminescence bioimaging showed time-dependent lung metastatic growth of control cells but no growth (or a reduction in signals) with EHD2 KO cells (**Fig. 4A-C**). These findings were confirmed by assessment of lung metastatic nodules at necropsy (**Fig. 4D**). H&E and human CK18 staining confirmed the metastatic growths, and EHD2 expression pattern was confirmed by IHC (**Fig. 4E**). Collectively, our analyses definitively demonstrate a positive role of EHD2 in tumorigenic and pro-metastatic behavior in TNBC.

EHD2 and CAV1/2 are co-overexpressed in basal-like breast cancer and loss of EHD2 reduces the cell surface caveolae: EHD2 localizes to and is required for the stability of the cell surface caveolae (2, 3, 8, 25). The bc-GenExMiner analysis of 5,277 BC samples (26) demonstrated tight co-expression of EHD2 with the structural components of caveolae, CAV1 and CAV2 in TNBC samples (**Fig. 5A, Supplementary Fig. S5A**). By KM Plotter analysis, combined EHD2-, CAV1- and CAV2-high basal (PAM50-based) but not all BC patients showed significantly shorter distal metastasis-free survival (**Fig. 5B, Supplementary Fig. S5B**). Immunoblotting demonstrated concordant EHD2 and CAV1 expression in mammary epithelial and BC cell lines (**Fig. 5C**). Immunofluorescence analysis demonstrated a high degree of colocalization between EHD2 and CAV1 in TNBC cell lines (**Fig. 5D**). Total internal reflection fluorescence (TIRF) microscopy analysis of cell surface associated CAV1-GFP puncta, representing cell surface caveolae showed a significant reduction in EHD2 KO compared to control Hs578T cells (**Fig. 5E**), consistent with reported electron microcopy-based high cell surface caveolae density on Hs578T compared to a lower density on the EHD2-nonexpressing MDA-MB436 cells (8). CRISPR KO of CAV1 (**Fig. 5F**) led to a significant impairment of cell migration like that with EHD2 KO (**Fig. 5G**). These results support the conclusion that EHD2-dependent maintenance of cell surface caveolae is linked to its promotion of tumorigenic and pro-metastatic traits.

EHD2 promotes pro-metastatic traits in TNBC cells by upregulating store-operated calcium entry

Impact of EHD2 depletion on multiple oncogenic traits and its regulation of plasma membrane caveolae suggested the role for a caveolae-linked signaling machinery. We

investigated the linkage of EHD2 to store-operated calcium entry (SOCE) (27), a pathway that operates at caveolae (28, 29) and is a well-established pro-metastatic signaling pathway in TNBC and other cancers (17, 18). SOCE is mediated by the translocation of the endoplasmic reticulum (ER) Ca^{2+} sensor to ER-plasma membrane contact sites upon ER Ca^{2+} depletion which permits its binding to and activation of the Orai1 membrane Ca^{2+} channel to promote Ca^{2+} entry for Ca^{2+}-dependent signaling and refilling of the ER (27).

To examine if EHD2 regulates SOCE in TNBC cells, calcium-sensitive fluorescent dye (Fluo4 AM)-loaded cells in Ca^{2+} free medium were treated with thapsigargin (Tg), an inhibitor of the ER-localized Sarco-Endoplasmic Reticulum Ca^{2+} ATPase 2 (SERCA-2) (30). Expectedly, control Hs578T or BT549 TNBC cells exhibited a robust rise in cytoplasmic Ca^{2+} that declined over time (**Fig. 6A-B**), reflecting the release of ER Ca^{2+} (31). Subsequent addition of Ca^{2+} in the medium induced a rapid increase in cytoplasmic Ca^{2+}, indicating the SOCE (**Fig. 6A-B**) (31). Pre-treatment with the SOCE inhibitor SKF96365 (18) markedly reduced the initial Ca^{2+} flux and nearly abrogated the SOCE (**Fig. 6C**. EHD2 KO cells demonstrated a marked defect in both the initial Tg-induced rise in cytoplasmic Ca^{2+} and the subsequent SOCE (**Fig. 6A-B**). Defective SOCE was also seen in EHD2 KO Hs578T cells using another SERCA inhibitor cyclopiazonic acid (CPA) (32) (**Fig. 6D**). In a genetic approach, we showed that EHD2 KO Hs578T cells stably expressing a GFP-based reporter of cytoplasmic Ca^{2+}, GCaMP6s, (33), exhibited defective Tg-induced SOCE (**Fig. 6E**, **Supplementary Fig. S6A**). Further, stable expression of GCaMP6s-CAAX, a plasma membrane-targeted fluorescent reporter of Ca^{2+} levels (34), which only detects the SOCE phase upon Tg treatment directly established the defective SOCE in EHD2-KO Hs578T cells (**Fig. 6F**, **Supplementary Fig. S6B**). In a reciprocal experiment, CRISPRa-induced endogenous EHD2 expression in EHD2-negative MDA-MB468 cells led to a marked

increase in Tg-induced SOCE (**Fig. 6G**). Consistent with the role of caveolae, a marked defect in SOCE was observed in CAV1-KO TNBC cell lines (**Fig. 6H-I**).

Next, we transiently transfected the CFP-tagged STIM1 in control or EHD2 KO Hs578T cells and quantified the number of fluorescent STIM1 puncta at the cell surface, a measure of STIM1-Orai1 interaction, using TIRF microscopy (35). Tg treatment failed to increase the STIM1 puncta in EHD2 KO cells (**Fig. 7A**). This defect was not a result of reduced levels of total STIM1 and Orai1 proteins (**Fig. 7B**). Given the known localization of Orai1 in caveolae (29, 36), we assessed the impact of EHD2 KO on Oraai1 cell surface levels. We used an anti-Orai1 antibody authenticated against control or Orai1 knockdown TNBC cell lines (**Supplementary Fig. S7**) to immunoprecipitate Orai1 from surface biotin-labeled control and EHD2 KO MDA-MB-231 or Hs578T cells and confirmed the comparable immunoprecipitation of total Orai1 in WT vs. KO cells (**Fig. 7C, upper panels**). In contrast, streptavidin blotting revealed a marked reduction in biotinylated (cell surface) Orai1 signals in EHD2 KO cells (**Fig. 7C, lower panels**). Further linking the SOCE to EHD2-dependent pro-metastatic traits, overexpression of CFP-STIM1 in EHD2-KO Hs578T cells (**Fig. 7D**) partially rescued the SOCE defect (**Fig. 7E**) and the defective cell migration (**Fig. 7F**). In a complementary approach, the tool SOCE inhibitor SKF96365 and a recently identified inhibitor CM4620, which (as Auxora^{TM}; Calcimedica) has progressed to phase 3 clinical trials in acute inflammatory disease conditions (37), impaired the SOCE in wildtype TNBC cells and further reduced the residual SOCE in EHD2-KO cells (**Fig. 6C**). These SOCE inhibitors significantly impaired the wildtype TNBC cell migration, and further reduced the migration of EHD2 KO cells, albeit it was not statistically significant (**Fig. 8A**). Thus, a major proportion of the SOCE in TNBC cell lines is dependent on EHD2 and is inhibitable with available SOCE inhibitors. Accordingly, we show that SKF96365 treatment

significantly reduced the control TNBC xenograft tumor growth (**Fig. 8B**); the EHD2 KO xenografts as these did not grow sufficiently to test the impact of SOCE inhibition. Collectively, these findings support our conclusion that EHD2, by stabilizing caveolae, facilitates the SOCE to promote downstream pro-oncogenic traits in TNBC cells.

Discussion:

Elucidating novel tumorigenesis- and metastasis-associated cellular adaptations could dictate new therapeutic options in BC. Here, we use TNBC cell models to elucidate a novel signaling axis linking EHD2 overexpression in BC to store-operated calcium entry (SOCE), a known pro-oncogenic and pro-metastatic pathway. Our studies support the potential for targeting the SOCE pathway in EHD2-overexpressing TNBC and other BC subtypes.

Our IHC analyses demonstrated high cytoplasmic EHD2 expression in a substantial proportion of breast tumors, associated with shorter BC-specific patient survival (**Fig. 1B**) and higher tumor grade (**Supplementary Table 1**). A higher proportion of TNBC and HER2+ patients exhibited high cytoplasmic EHD2 (**Fig. 1C, Supplementary Table 1**). Our results differ from reported reduction in EHD2 expression correlates with tumor progression in BC (11, 22). Notably, a recent study, while it reported the depletion of EHD2 to an increase the oncogenic traits of BC cell lines, found low EHD2 expression in breast tumors to specify good prognosis and better chemotherapy response (16). Several factors could account for the discordance, including the lack of antibody validation of antibodies in prior studies, the high EHD2 expression in normal mammary adipocytes (**Supplementary Fig. S1A-B**), resulting in apparent reduction in EHD2 expression in tumor tissue using western blotting (11, 16, 22), and the possibility that EHD2 signals in prior studies represented nuclear EHD2, which we find is

associated with positive prognostic factors (**Fig. 1B, Supplementary Table 1**). Notably, mechanical stimuli were reported to promote the nuclear translocation of EHD2 (8) but any link of the nuclear/cytoplasmic partition of EHD2 to oncogenesis is currently unknown.

Analysis of mRNA expression in public BC databases (**Fig. 5A**) and of protein levels in BC cell lines (**Fig. 5C**) demonstrated high degree of EHD2 co-expression with caveolin-1/2, the structural elements of caveolae. This was noteworthy since EHD2 regulates the stability of caveolae (2, 3). Significantly, EHD2 and/or caveolin-1/2 mRNA overexpression predicted shorter patient survival specifically in the PAM50-defined basal BC (**Fig. 5B**), consistent with the predominant basal (myoepithelial) cell expression of EHD2 in mouse mammary epithelium (**Supplementary Fig. S1B, 1D**). Thus, high EHD2 expression is a feature of BC with basal-like features.

Multi-pronged approaches using shRNA knockdown and CRISPR-Cas9 KO of EHD2 in TNBC cell models together with mouse rescue of EHD2-KO demonstrated that EHD2 is required for tumorigenesis and metastasis. We show that in vitro tumor cell growth under stringent conditions (tumorsphere) (**Fig. 2C**) and pro-metastatic traits of cell migration, invasion, and ECM degradation (**Fig. 2D, 3B, 3D**) are EHD2-dependent. In vivo, loss of EHD2 markedly impaired orthotopic TNBC xenograft formation and metastasis (**Fig. 2F; Fig. 3H**), and tumor growth was rescued by exogenous mouse EHD2 (**Fig. 3H**). Notably, intravenous injections demonstrated the inability of EHD2-KO TNBC cells to form lung metastases (**Fig. 4A-C**). Collectively, our analyses conclusively demonstrate that EHD2 overexpression in BC cells represents a key pro-tumorigenic and pro-metastatic adaptation.

Mechanistically, we link the EHD2 overexpression in BC cells to regulation of caveolae, whose stability is known to be controlled by EHD2 (2, 3, 20). This includes the strong EHD2 co-

localization with CAV1/2 (**Fig. 5D**), reduction in cell surface caveolae density using TIRF microscopy upon EHD2 KO (**Fig. 5E**), and inhibition of TNBC cell migration upon CAV1 KO (**Fig. 5G**), consistent with the previously documented pro-tumorigenic roles of CAV1 in TNBC (38, 39).

Caveolae serve as hubs for signaling (40). Among these, the SOCE pathway stood out as it is known to regulate multiple tumorigenic and pro-metastatic traits in TNBC (28, 29), as with EHD2 depletion. Also, EHD2 interacts with Ca^{2+}-binding proteins such as Ferlins (41) that are involved in Ca^{2+}-dependent membrane repair and EHD2 was found to accumulate at sites of membrane repair in skeletal muscle models (42, 43). Indeed, our extensive analyses demonstrate that EHD2 is a major positive regulator of SOCE in TNBC cell models. This includes analyses of fluorescent dye-labeled cells and two distinct agents (thapsigargin or CPA) to release ER Ca^{2+} as stimuli (**Fig. 6A-B**), and independent validation using cytoplasm- or plasma membrane-localized genetic reporters of Ca^{2+} (**Fig. 6E-F**, Supplementary **Fig. S6A-B**). Reciprocally, CRISPR-activation of endogenous EHD2 expression in an EHD2-nonexpressing TNBC cell line upregulated SOCE (**Fig. 6G**) and cell migration (**Fig. 3G**). Complementing these, EHD2 KO reduces the STIM1-Orai1 interaction at the ER-plasma membrane contact sites as measured using fluorescent STIM1 (**Fig. 7A**) and overexpression of STIM1 partially rescues the SOCE and cell migration defects in EHD2-KO TNBC (**Fig. 7E-F**).

Orai1 is a major STIM1-interacting caveolae-resident SOCE channel (29, 36). Indeed, our cell surface biotinylation studies demonstrated that EHD2 KO specifically reduces the cell surface Orai1 levels (**Fig. 7C**). Thus, our findings support a model whereby EHD2-dependent stabilization of cell surface caveolae ensures high cell surface levels of Orai1 to enable robust SOCE in TNBCs, which in turn promotes pro-tumorigenic and pro-metastatic behaviors of tumor

cells (17, 18). Consistent with this model, EHD2 deficiency reduced the cell surface levels of caveolae-associated ATP-sensitive K^+ channels (6).

Finally, consistent with prior studies (18), chemical inhibition of SOCE markedly impaired the pro-metastatic traits of EHD2-overexpressing TNBCs, with a smaller impact on EHD2 KO cell lines (**Fig. 8A**), and impaired the TNBC metastatic growth in vivo (**Fig. 8B**). Together, our studies support the idea that EHD2-overexpressing subsets of TNBC and other BC subtypes may be selectively amenable to SOCE targeting, with EHD2 and CAV1/2 overexpression as predictors of response.

Materials and methods

Detailed Materials and Methods of the following sections are included in Supplementary Information.

Patient population and tissue microarrays, prognostic analysis and gene targeted correlation analysis of *EHD2, CAV1* and *CAV2* mRNAs, cell lines and media, antibodies and reagents, transfection reagents and plasmids, generation of shRNA knockdown and CRISPR-Cas9 knockout/activation cell lines**,** cell lysates preparation, immunoprecipitation assay, immunofluorescence microscopy, proliferation assay, extracellular matrix degradation assay**,** anchorage-independent growth assay, tumor-sphere assay, Matrigel spheroid invasion assay, trans-well migration and invasion assays, orthotopic xenograft tumorigenesis, and analysis of tumor metastasis after tail vein injection of tumor cells.

TIRF microscopy: Cells were seeded on 1.78 refractive index glass coverslips and transfected with pGFP-CAV1 (for CAV1 puncta) or STIM1-CFP (for STIM1 puncta). Cells were treated

with or without thapsigargin (2.5uM) before imaging. TIRF images were acquired using a TIRF video microscope (Nikon) equipped with CFI Apo TIRF 100A- NA 1.49 oil objective and an EMC CD camera (Photometrics HQ2). The surface CAV1 puncta were quantified using the ImageJ (NIH) software.

Live-cell surface biotin labeling to assess the cell surface Orai1 levels: Cell monolayers were washed with ice-cold PBS, and incubated in the same buffer containing sulfo-NHS-LC-biotin (#A39257, ThermoFisher) for 30 min at 4°C. The cells were washed in PBS and their lysates in TX-100 lysis buffer subjected to anti-Orai1 immunoprecipitation followed by blotting with Streptavidin-Horseradish Peroxidase (HRP) Conjugate (cat. # SA10001) and enhanced chemiluminescence detection.

Calcium flux assays: Cells were seeded in 35-mm glass-bottom dishes (cat. #FD35-100, WPI Inc) and loaded with Fluo4-AM in modified Tyrode's solution (2 mM calcium chloride, 1 mM magnesium chloride, 137 mM sodium chloride, 2.7 mM potassium chloride, 12 mM sodium bicarbonate, 0.2 mM sodium dihydrogen phosphate, 5.5 mM glucose, pH 7.4) for 1 hour. After washing with calcium-free Tyrode's solution, live cells were imaged under a confocal microscope (LSM710; Carl Zeiss), with fluorescence excitation at 488 nm and emission at 490–540 nm. To initiate the release of intracellular Ca2+ stores, cells were stimulated with 2.5 μM thapsigargin in the absence of extracellular Ca^{2+}. Once the signals approached the baseline, calcium chloride was added to 2 mM final concentration to record the SOCE (44). Data are presented as fold change in fluorescence emission relative to baseline.

Statistical analysis: Statistical analysis of in vitro data was performed by comparing groups using unpaired student's t test. In vivo tumorigenesis and metastasis data were analyzed using two-way ANOVA. A p value of <0.05 was considered significant.

Human and animal subjects: The Ethics Committee of University of Nottingham approved the use of human tissues. All mouse xenograft and treatment studies were pre-approved by the UNMC Institutional Animal Care and Use Committee (IACUC) and conducted strictly according to the pre-approved procedures, in compliance with Federal and State guidelines.

Author contributions

Designing research studies: H.B., V.B., H.L., T.A.B., DWC; Conducting experiments: H.L., T.A.B., B.C.M., N.I., I.M., A.M.B., S.C., M.R., W.B.T.; Acquiring and analyzing data: H.L., T.A.B., B.C.M., S.M., J.L.M., E.A.R.; Providing reagents: M.D.S.; Writing the manuscript: H.B., H.L., T.A.B., B.C.M. All authors have read and agreed to the final manuscript.

Acknowledgements: We thank Drs. Anjana Rao for CFP-STIM1, Ari Helenius for Cav1-EGFP and Ian Frew for the pMule kit (used to assemble the tdTomato/luciferase) through Addgene. This research was funded by grants from DOD (W81XWH-17-1-0616 and W81XWH-20-1-0058 to HB and W81XWH-20-1-0546 to VB) and NIH (R21CA241055 and R03CA253193 to VB), and by Fred & Pamela Buffett Cancer Center (pilot grants to HB & VB) and the Raphael Bonita Memorial Fund. The UNMC core facilities are supported by the NCI Cancer Center Support Grant (P30CA036727) to Fred & Pamela Buffett Cancer Center and the Nebraska Research

Initiative. TAB, AMB and SC received University of Nebraska Medical Center Graduate Student Fellowships.

Figure Legends

Figure 1. EHD2 is overexpressed in a subset of breast cancer patients and is associated with metastasis and shorter survival. (A) Representative images of negative/low/high cytoplasmic and nuclear EHD2 IHC staining of a breast cancer tumor microarray (840 samples). (B) Kaplan-Meier survival curves correlating positive/high (green) vs low/negative (blue) nuclear (left panel; N=288/458) or cytoplasmic (right panel; N=392/352) EHD2 expression with Breast Cancer Specific Survival (BCSS). (C) Number (Y-axis) and % (within bars) cytoplasmic EHD2-negative/low (gray) and -positive/high samples among ER/PR+, ErbB2+, TN, and all tumors.

Figure 2. EHD2 knockdown in TNBC cell lines impairs the tumorigenic and pro-metastatic traits. (A) Immunoblot confirmation of shRNA-mediated EHD2 knockdown. (B) Cell Titer-Glo proliferation (2,000 cells/well; 24 replicates each) over time. Mean +/- SEM, n=3, ns, not significant. (C) Tumorsphere formation quantified on day 7. Left, representative images; Right, quantification of tumorspheres/well. Mean +/- SEM, n=3, *p<0.05; **p<0.01. (D) Transwell invasion of cells plated in 0.5% FBS medium towards complete medium assayed after 18h. Left, representative images; Right, quantification of invaded cells (Mean +/- SEM, n=3, *p<0.05). (E) Three-dimensional invasion in Matrigel-grown organoids. 2,000 cells plated per well in 50% Matrigel on top of 100% Matrigel layer in 8-well chamber slides for 7 days before imaging. Left, representative images; right, % spheroids with invasive fronts from over 100 counted per well, n=4, *** p<0.001). (F) Xenograft tumorigenesis. 4-weeks old nude mice orthotopically-injected with $5x10^6$ cells were followed over time. Left, fold change in tumor volume over time for individual mice. Mean (red/blue lines) +/- SEM; ****,p<0.0001 by two-way ANOVA. Right,

representative tumors (close to median of groups). (G, H) Representative IHC staining of tumor sections for EHD2 (G) or Ki67 (H), with respective controls. Right, Mean +/- SEM of Ki67+ staining. ****, p<0.0001.

Figure 3. EHD2 knockout in TNBC cell lines impairs the tumorigenic and pro-metastatic traits. Single cell clones of TNBC cell lines serially transduced with Cas9 and control or EHD2 sgRNA lentiviruses were obtained and use as a pool of >3 clones. (A) Immunoblotting of EHD2 expression in KO vs. WT (Cas9) controls. (B) Transwell migration. Data points are independent experiments; Mean +/- SEM of migrated cells (input 10K), **p<0.01, *p<0.05. (C) Transwell invasion across Matrigel. Mean +/- SEM of invaded cells (input 10K), **p<0.01, *p<0.05. (D) Extracellular matrix degradation. Cells plates on Cy5-gelatin and percentage area with matrix degradation quantified after 48h. Mean +/- SEM, **p<0.01. (E) Mouse EHD2 rescue of EHD2 KO MDA-MB-231 cells. Left, immunoblot to show re-expression of mouse EHD2; beta-actin, loading control. Right, rescue of cell migration defect. Mean +/- SEM, ***p<0.001, **p<0.01, *p<0.05. (F-G) CRISPRa induction of endogenous EHD2 expression in EHD2-negative MDA-MB-468 cell line (F) and increase in migration (G). Mean +/- SEM, *p<0.05. (H) Impairment of tumorigenesis by EHD2 KO and rescue by mouse EHD2 reconstitution. Left, groups of 8 nude mice orthotopically implanted with $3x10^6$ cells and tumors analyzed as in Fig. 2F: ****p<0.0001, **p=0.001. Right, Representative tumor images. Bottom, representative tumor sections stained for EHD2 and control.

Figure 4: EHD2 KO impairs the ability of TNBC cells to form lung metastases. WT control and EHD2 KO MDA-MB-231 cells were engineered with tdTomato-luciferase and 10^6 cells of each injected intravenously into groups of 7 nude mice. Lung metastases were monitored by bioluminescence imaging (shown in A). (B-C) Bioluminescence signals over time (Control, blue; KO, red) are shown as either untransformed photon flux values (B) or log fold-change in photon flux relative to day 0 (C). Two-way ANOVA showed the differences between Control and KO groups to be significant (*$p<0.05$). (D) Left panel, images of lungs harvested at necropsy show nearly complete absence of metastatic nodules in lungs of mice injected with EHD2 KO cells. Right panel, quantification of tumor nodules in the lungs, **, $p<0.01$. (E) Representative H&E (first panels), EHD2 (second panels), CK18 (third panels) and control IgG staining of metastatic lung tissue sections from control (upper) and EHD2 KO cell injected mice. Note the retention of normal lung tissue in EHD2 KO cell injected mouse lung, and absence of EHD2 expression in KO nodules (labeled M). CK18 demarcates the human tumor cell area.

Figure 5. EHD2 and Caveolin-1/2 are co-overexpressed in breast cancers and EHD2 regulates cell surface caveolae. (A) Pearson's correlation plots of EHD2/CAV1 and EHD2/CAV2 expression in TNBC (IHC-based) subsets of TCGA and SCAN-B RNAseq datasets analyzed on bc-GenExMiner v4.5 platform. Indicated: n, number of samples; R, correlation coefficients; significance. (B) KM plotter analysis of EHD2, CAV1 and CAV2 overexpression correlation with relapse-free survival (RFS) for upper vs. lower quartiles in basal-like breast cancer (PAM50-based) cohorts of TCGA, GEO and GEA datasets. Probe sets used: EHD2 (221870_at), CAV1 (212097_at) and CAV2 (203323_at). Analysis of all samples combined found no survival differences (lower panel). (C) Immunoblot analysis of coordinate

EHD2 and CAV1 expression in immortal mammary epithelial cells and breast cancer cell lines. (D) Immunofluorescence colocalization of EHD2 (red) and caveolin-1 (green) in TNBC cell lines; scale bar, 100 μm. (E) TIRF analysis of fluorescent CAV1 puncta to quantify cell surface caveolae pool. Top, representative TIRF images. Bottom, quantification of CAV1 puncta. Mean +/- SEM of puncta per cell pooled from 3 independent experiments; **p<0.01. (F) Immunoblot confirmation of CRISPR-Cas9 CAV1 KO in TNBC cell lines. (G) Impact of CAV1 KO on Transwell migration. Mean +/- SEM number of migrated cells (input 10K) per Transwell (n=3, *p<0.05).

Figure 6. EHD2 promotes store-operated calcium entry (SOCE) in TNBC cell lines. (A-B) Thapsigargin (Tg; 2.5 uM)-induced increase in cytoplasmic Ca^{2+} (initial rise in no extracellular Ca^{2+}) and SOCE (second peak after adding 2 mM Ca^{2+}) in Fluo 4 AM-loaded WT/KO Hs578T (A) or BT549 (B) cell lines measured by live-cell confocal microscopy. (C) Impact of SOCE inhibitor SKF96365 (10 μM) on Tg (2.5 uM)-induced Ca^{2+} fluxes measured as in A. (D) Defective Tg-induced Ca^{2+} fluxes demonstrated using cyclopiazonic acid (CPA; 1 μM). (E-F) Tg (2.5 uM)-induced Ca^{2+} fluxes measured by confocal imaging of stably-expressed genetic cytoplasmic Ca^{2+} sensors: cytoplasmic sensor GCaMP6s (E) and plasma membrane-localized sensor GCaMP6s-CAAX (F). (G) Tg (2.5 uM)-induced Ca^{2+} fluxes in Fluo4 AM-loaded control MDA-MB468 (EHD2-negative) vs its CRSIPRa derivative (EHD2-expressing). (H-I) Tg (2.5 uM)-induced Ca^{2+} fluxes in Fluo4 AM-loaded control and CAV1 KO TNBC lines. Mean +/- SEM of peak fluorescence intensity (n=3, *p<0.05) is shown below all panels.

Figure 7. EHD2 regulates SOCE through STIM1-Orai1. (A) CFP-STIM1-trasnfected cells were analyzed for plasma membrane proximal fluorescent puncta by TIRF microscopy, without (control) or with thapsigargin treatment (2.5 μM, 5 min). Left, representative TIRF images; Right, Mean +/- SEM of STIM1 puncta/cell, ** $p<0.01$. (B) Immunoblotting to show comparable total STIM1 and Orai1 levels in control vs EHD2 KO TNBC lines; Hsc70, loading control. (C) Reduced cell surface levels of Orai1 in EHD2 KO cells. Live cell surface biotinylated cell Orai-1 immunoprecipitates blotted with Streptavidin (top) and Orai1 (bottom). (D) Anti-STIM1 immunoblotting to show stable overexpression of STIM1-CFP in EHD2 KO Hs578T cells. (E) Partial rescue of SOCE by ectopic CFP-STIM1 overexpression analyzed upon thapsigargin (Tg; 2.5uM) treatment of Fluo 4 AM-loaded cells. Bottom, Mean +/- SEM of peak fluorescence, N=3; *$p<0.05$. (F) Partial rescue of Transwell cell migration defect by CFP-STIM1 overexpression in EHD2 KO cells. Mean +/- SEM of migrated cells (input 10K); n=3; *$P<0.05$.

Figure 8. EHD2 expression determines the relative functional impact of SOCE inhibition in TNBC cells. (A) Impact of SOCE inhibitors SKF96365 (10 μM) or CM4620 (10 μM) Transwell migration of Control vs EHD2 KO TNBC cell lines. Mean +/- SEM of n=3; ***$P<0.001$. (B) SOCE inhibition reduces TNBC tumorigenesis. Nude mice (8/group) bearing orthotopic MDA-MB-231 ($3x10^6$) cell tumors (average 4-5 mm in diameter) were administered 10 mg/kg SKF96365 (in PBS) or PBS intraperitoneally and change in tumor volumes (V_t/V_0) monitored over time and differences analyzed by two-way ANOVA. Right, representative tumor images.

References

1. Naslavsky N, Caplan S. EHD proteins: Key conductors of endocytic transport. Trends Cell Biol 2011;21:122-31.

2. Moren B, Shah C, Howes MT, Schieber NL, McMahon HT, Parton RG, et al. EHD2 regulates caveolar dynamics via ATP-driven targeting and oligomerization. Mol Biol Cell 2012;23:1316-29.

3. Stoeber M, Stoeck IK, Hanni C, Bleck CK, Balistreri G, Helenius A. Oligomers of the ATPase EHD2 confine caveolae to the plasma membrane through association with actin. EMBO J 2012;31:2350-64.

4. Matthaeus C, Lahmann I, Kunz S, Jonas W, Melo AA, Lehmann M, et al. EHD2-mediated restriction of caveolar dynamics regulates cellular fatty acid uptake. Proc Natl Acad Sci U S A 2020;117:7471-81.

5. Matthaeus C, Lian X, Kunz S, Lehmann M, Zhong C, Bernert C, et al. eNOS-NO-induced small blood vessel relaxation requires EHD2-dependent caveolae stabilization. PLoS One 2019;14:e0223620.

6. Yang HQ, Jana K, Rindler MJ, Coetzee WA. The trafficking protein, EHD2, positively regulates cardiac sarcolemmal K(ATP) channel surface expression: Role in cardioprotection. FASEB J 2018;32:1613-25.

7. Sinha B, Koster D, Ruez R, Gonnord P, Bastiani M, Abankwa D, et al. Cells respond to mechanical stress by rapid disassembly of caveolae. Cell 2011;144:402-13.

8. Torrino S, Shen WW, Blouin CM, Mani SK, Viaris de Lesegno C, Bost P, et al. EHD2 is a mechanotransducer connecting caveolae dynamics with gene transcription. J Cell Biol 2018;217:4092-105.

9. Li M, Yang X, Zhang J, Shi H, Hang Q, Huang X, et al. Effects of EHD2 interference on migration of esophageal squamous cell carcinoma. Med Oncol 2013;30:396,012-0396-4. Epub 2013 Jan 25.

10. Guan C, Lu C, Xiao M, Chen W. EHD2 overexpression suppresses the proliferation, migration, and invasion in human colon cancer. Cancer Invest 2021;39:297-309.

11. Yang X, Ren H, Yao L, Chen X, He A. Role of EHD2 in migration and invasion of human breast cancer cells. Tumour Biol 2015;36:3717-26.

12. Liu J, Ni W, Qu L, Cui X, Lin Z, Liu Q, et al. Decreased expression of EHD2 promotes tumor metastasis and indicates poor prognosis in hepatocellular carcinoma. Dig Dis Sci 2016;61:2554-67.

13. Zhang Z, Chen J, Huo X, Zong G, Huang K, Cheng M, et al. Identification of a mesenchymal-related signature associated with clinical prognosis in glioma. Aging (Albany NY) 2021;13:12431-55.

14. Kim Y, Kim MH, Jeon S, Kim J, Kim C, Bae JS, et al. Prognostic implication of histological features associated with EHD2 expression in papillary thyroid carcinoma. PLoS One 2017;12:e0174737.

15. Liu C, Liu S, Wang L, Wang Y, Li Y, Cui Y. Effect of EH domain containing protein 2 on the biological behavior of clear cell renal cell carcinoma. Hum Exp Toxicol 2019;38:927-37.

16. Shen WW, Bièche I, Fuhrmann L, Vacher S, Vincent-Salomon A, Torrino S, et al. EHD2 is a predictive biomarker of chemotherapy efficacy in triple negative breast carcinoma. Sci Rep 2020;10:7998,020-65054-5.

17. Mo P, Yang S. The store-operated calcium channels in cancer metastasis: From cell migration, invasion to metastatic colonization. Front Biosci (Landmark Ed) 2018;23:1241-56.

18. Yang S, Zhang JJ, Huang XY. Orai1 and STIM1 are critical for breast tumor cell migration and metastasis. Cancer Cell 2009;15:124-34.

19. George M, Ying G, Rainey MA, Solomon A, Parikh PT, Gao Q, et al. Shared as well as distinct roles of EHD proteins revealed by biochemical and functional comparisons in mammalian cells and C. elegans. BMC Cell Biol 2007;8:3.

20. Morén B, Hansson B, Negoita F, Fryklund C, Lundmark R, Göransson O, et al. EHD2 regulates adipocyte function and is enriched at cell surface-associated lipid droplets in primary human adipocytes. Mol Biol Cell 2019;30:1147-59.

21. Zhao X, Malhotra GK, Lele SM, Lele MS, West WW, Eudy JD, et al. Telomerase-immortalized human mammary stem/progenitor cells with ability to self-renew and differentiate. Proc Natl Acad Sci U S A 2010;107:14146-51.

22. Shi Y, Liu X, Sun Y, Wu D, Qiu A, Cheng H, et al. Decreased expression and prognostic role of EHD2 in human breast carcinoma: Correlation with E-cadherin. J Mol Histol 2015;46:221-31.

23. Abd El-Rehim DM, Ball G, Pinder SE, Rakha E, Paish C, Robertson JF, et al. High-throughput protein expression analysis using tissue microarray technology of a large well-characterised series identifies biologically distinct classes of breast cancer confirming recent cDNA expression analyses. Int J Cancer 2005;116:340-50.

24. Cheung KJ, Ewald AJ. Illuminating breast cancer invasion: Diverse roles for cell-cell interactions. Curr Opin Cell Biol 2014;30:99-111.

25. Senju Y, Rosenbaum E, Shah C, Hamada-Nakahara S, Itoh Y, Yamamoto K, et al. Phosphorylation of PACSIN2 by protein kinase C triggers the removal of caveolae from the plasma membrane. J Cell Sci 2015;128:2766-80.

26. Jézéquel P, Frénel JS, Campion L, Guérin-Charbonnel C, Gouraud W, Ricolleau G, et al. Bc-GenExMiner 3.0: New mining module computes breast cancer gene expression correlation analyses. Database (Oxford) 2013;2013:bas060.

27. Chung WY, Jha A, Ahuja M, Muallem S. Ca(2+) influx at the ER/PM junctions. Cell Calcium 2017;63:29-32.

28. Pani B, Singh BB. Lipid rafts/caveolae as microdomains of calcium signaling. Cell Calcium 2009;45:625-33.

29. Bohorquez-Hernandez A, Gratton E, Pacheco J, Asanov A, Vaca L. Cholesterol modulates the cellular localization of Orai1 channels and its disposition among membrane domains. Biochim Biophys Acta Mol Cell Biol Lipids 2017;1862:1481-90.

30. Peterková L, Kmoníčková E, Ruml T, Rimpelová S. Sarco/Endoplasmic reticulum calcium ATPase inhibitors: Beyond anticancer perspective. J Med Chem 2020;63:1937-63.

31. Ong HL, Liu X, Sharma A, Hegde RS, Ambudkar IS. Intracellular ca(2+) release via the ER translocon activates store-operated calcium entry. Pflugers Arch 2007;453:797-808.

32. Demaurex N, Lew DP, Krause KH. Cyclopiazonic acid depletes intracellular Ca2+ stores and activates an influx pathway for divalent cations in HL-60 cells. J Biol Chem 1992;267:2318-24.

33. Chen TW, Wardill TJ, Sun Y, Pulver SR, Renninger SL, Baohan A, et al. Ultrasensitive fluorescent proteins for imaging neuronal activity. Nature 2013;499:295-300.

34. Tsai FC, Seki A, Yang HW, Hayer A, Carrasco S, Malmersjo S, et al. A polarized Ca2+, diacylglycerol and STIM1 signalling system regulates directed cell migration. Nat Cell Biol 2014;16:133-44.

35. Wu MM, Buchanan J, Luik RM, Lewis RS. Ca2+ store depletion causes STIM1 to accumulate in ER regions closely associated with the plasma membrane. J Cell Biol 2006;174:803-13.

36. Sathish V, Abcejo AJ, Thompson MA, Sieck GC, Prakash YS, Pabelick CM. Caveolin-1 regulation of store-operated ca(2+) influx in human airway smooth muscle. Eur Respir J 2012;40:470-8.

37. Bruen C, Al-Saadi M, Michelson EA, Tanios M, Mendoza-Ayala R, Miller J, et al. Auxora vs. placebo for the treatment of patients with severe COVID-19 pneumonia: A randomized-controlled clinical trial. Crit Care 2022;26:101,022-03964-8.

38. Badana A, Chintala M, Varikuti G, Pudi N, Kumari S, Kappala VR, et al. Lipid raft integrity is required for survival of triple negative breast cancer cells. J Breast Cancer 2016;19:372-84.

39. Zou M, Li Y, Xia S, Chu Q, Xiao X, Qiu H, et al. Knockdown of CAVEOLIN-1 sensitizes human basal-like triple-negative breast cancer cells to radiation. Cell Physiol Biochem 2017;44:778-91.

40. Lamaze C, Tardif N, Dewulf M, Vassilopoulos S, Blouin CM. The caveolae dress code: Structure and signaling. Curr Opin Cell Biol 2017;47:117-25.

41. Posey AD,Jr, Pytel P, Gardikiotes K, Demonbreun AR, Rainey M, George M, et al. Endocytic recycling proteins EHD1 and EHD2 interact with fer-1-like-5 (Fer1L5) and mediate myoblast fusion. J Biol Chem 2011;286:7379-88.

42. Marg A, Schoewel V, Timmel T, Schulze A, Shah C, Daumke O, et al. Sarcolemmal repair is a slow process and includes EHD2. Traffic 2012;13:1286-94.

43. Demonbreun AR, Quattrocelli M, Barefield DY, Allen MV, Swanson KE, McNally EM. An actin-dependent annexin complex mediates plasma membrane repair in muscle. J Cell Biol 2016;213:705-18.

44. Lu F, Sun J, Sun T, Cheng H, Yang S. Fluorescence-based measurements of store-operated ca(2+) entry in cancer cells using fluo-4 and confocal live-cell imaging. Methods Mol Biol 2018;1843:63-8.

Fig. 1

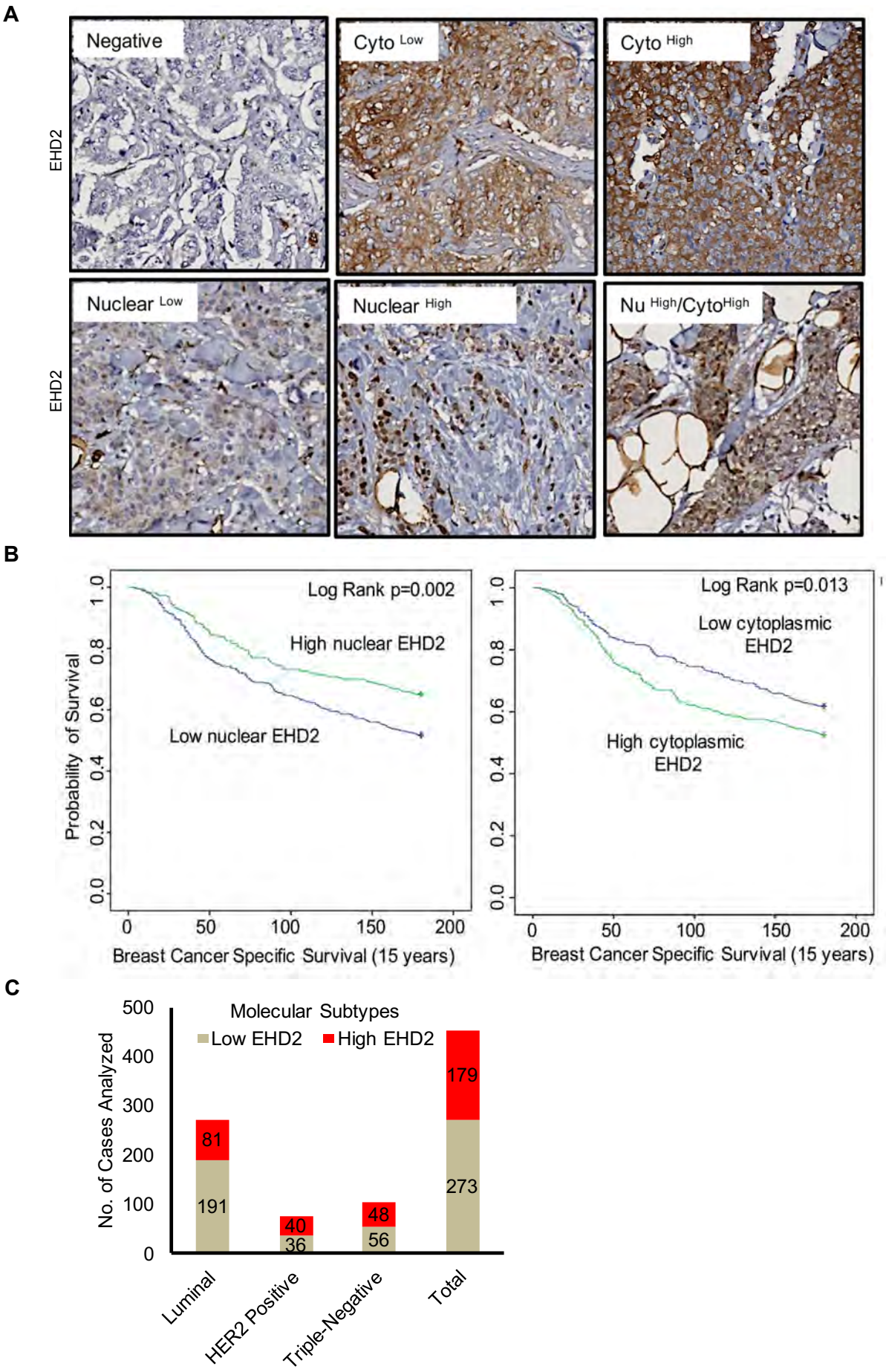
A
Negative
Cyto Low
Cyto High
EHD2
Nuclear Low
Nuclear High
Nu High/Cyto High
EHD2
B
Log Rank p=0.002
High nuclear EHD2
Low nuclear EHD2
Probability of Survival
0.0
0.2
0.4
0.6
0.8
1.0
0
50
100
150
200
Breast Cancer Specific Survival (15 years)
Log Rank p=0.013
Low cytoplasmic EHD2
High cytoplasmic EHD2
Breast Cancer Specific Survival (15 years)
C
Molecular Subtypes
Low EHD2
High EHD2
No. of Cases Analyzed
500
400
300
200
100
0
81
191
40
36
48
56
179
273
Luminal
HER2 Positive
Triple-Negative
Total

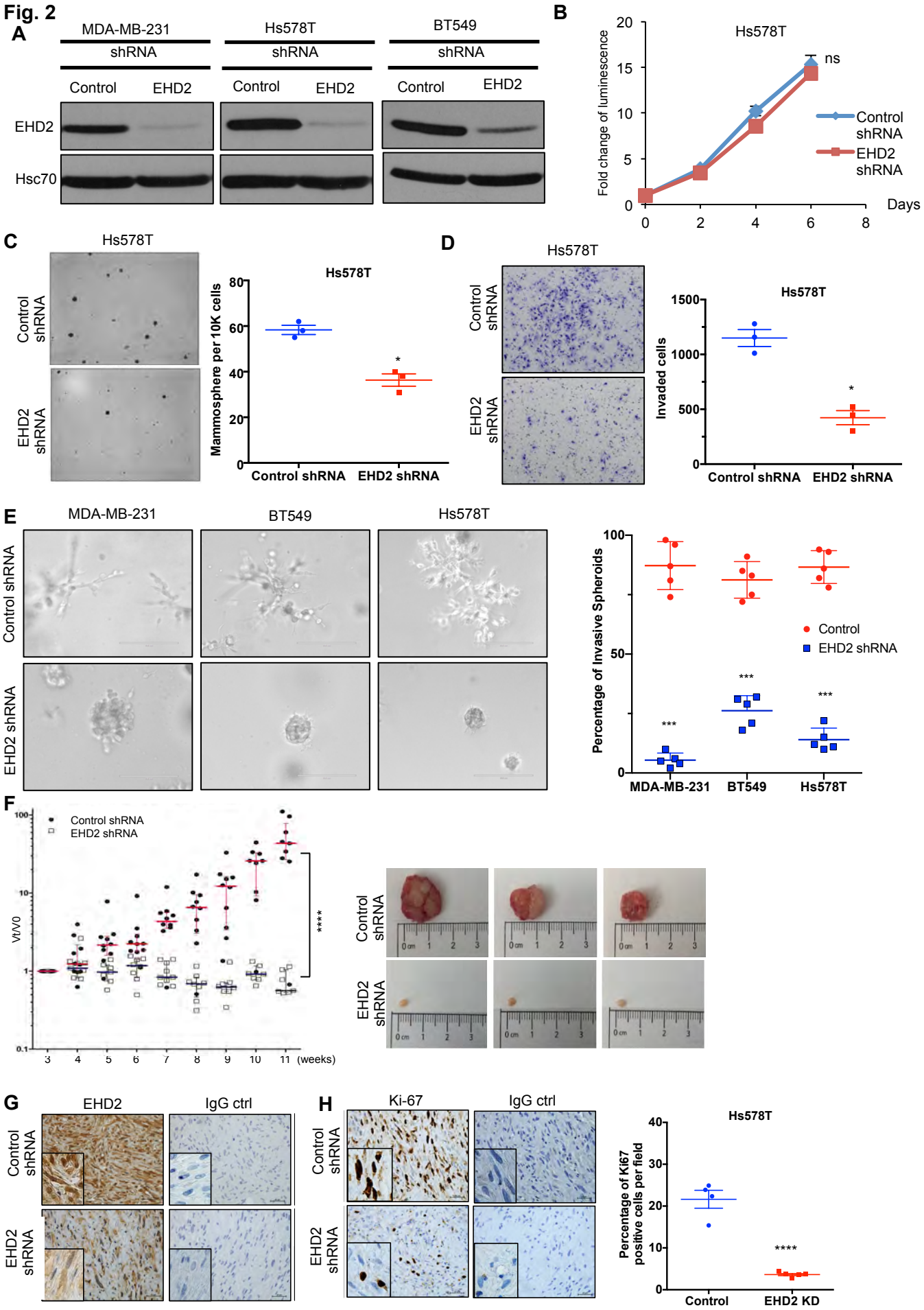
Fig. 2
A
MDA-MB-231
Hs578T
BT549
shRNA
Control
EHD2
EHD2
Hsc70
B
Hs578T
Fold change of luminescence
ns
Control shRNA
EHD2 shRNA
Days
C
Hs578T
Control shRNA
EHD2 shRNA
Mammosphere per 10K cells
D
Hs578T
Invaded cells
E
MDA-MB-231
BT549
Hs578T
Percentage of Invasive Spheroids
F
Control shRNA
EHD2 shRNA
Vt/V0
(weeks)
G
EHD2
IgG ctrl
H
Ki-67
IgG ctrl
Percentage of Ki67 positive cells per field
Control
EHD2 KD

Fig. 3

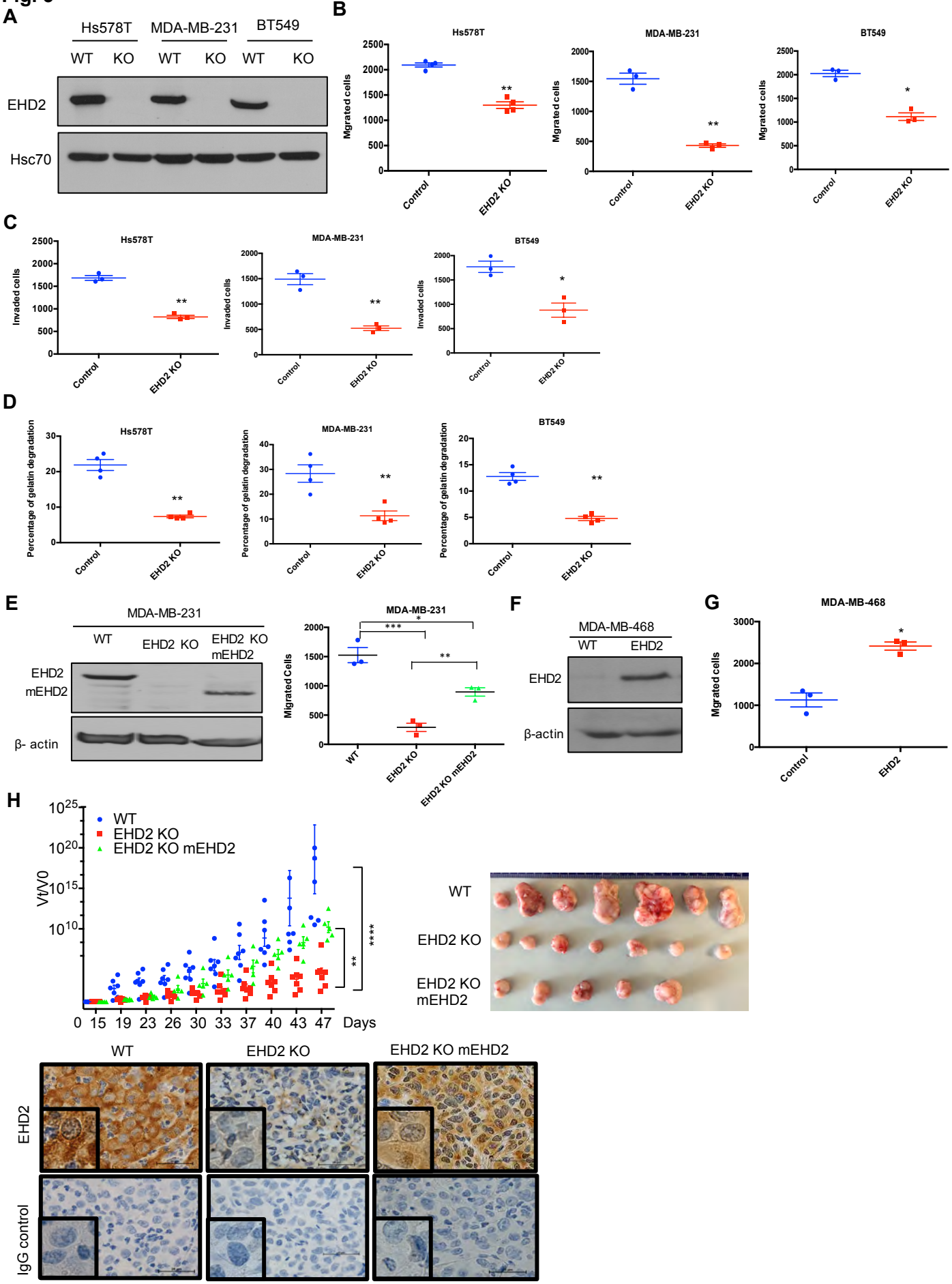
A
Hs578T
MDA-MB-231
BT549
WT
KO
EHD2
Hsc70
B
Hs578T
MDA-MB-231
BT549
Mgrated cells
Control
EHD2 KO
C
Invaded cells
D
Percentage of gelatin degradation
E
MDA-MB-231
WT
EHD2 KO
EHD2 KO mEHD2
EHD2
mEHD2
β- actin
Migrated Cells
F
MDA-MB-468
EHD2
β-actin
G
MDA-MB-468
Control
EHD2
H
WT
EHD2 KO
EHD2 KO mEHD2
Vt/V0
Days
IgG control

Fig. 4

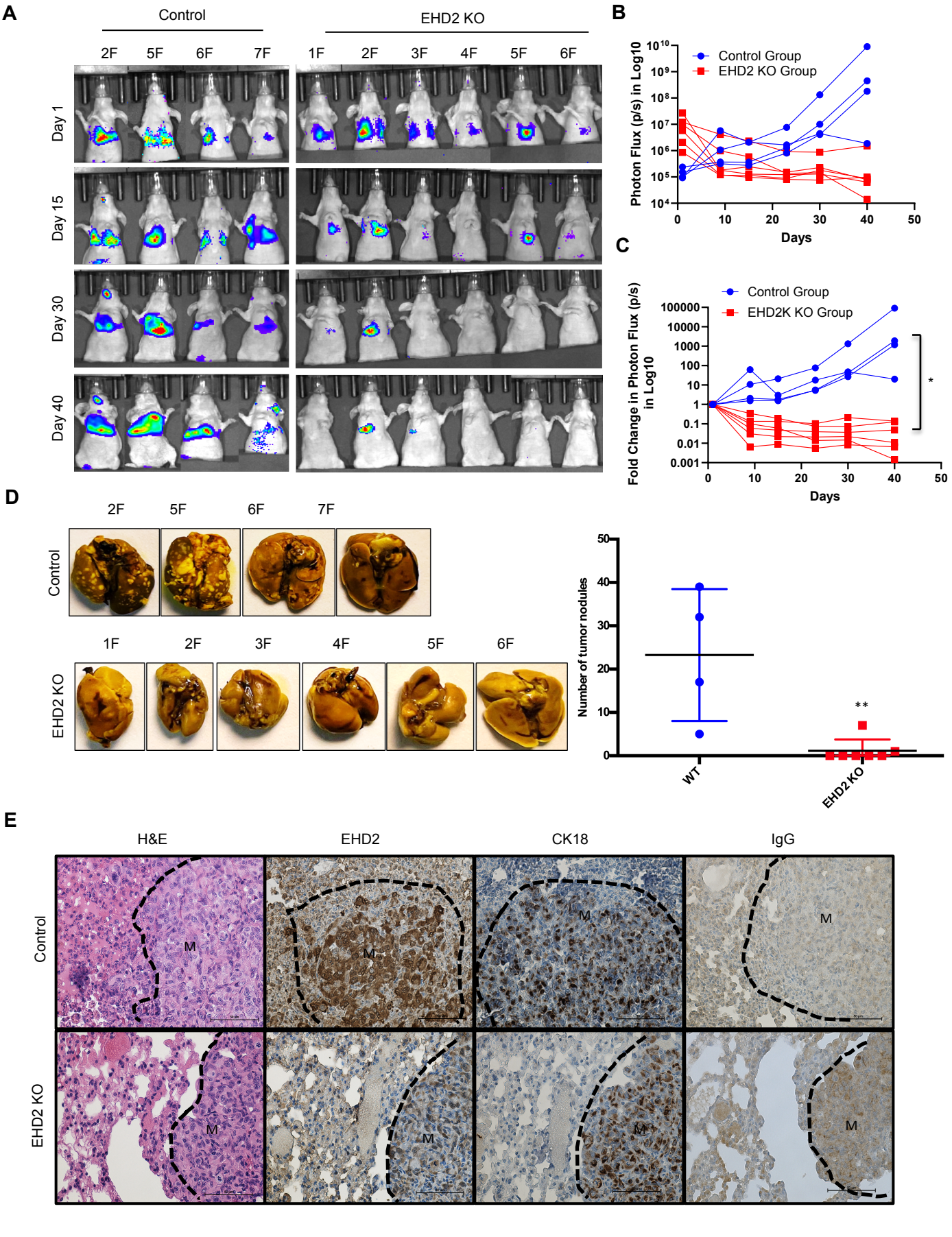
A
Control
EHD2 KO
2F
5F
6F
7F
1F
2F
3F
4F
5F
6F
Day 1
Day 15
Day 30
Day 40
B
Control Group
EHD2 KO Group
Photon Flux (p/s) in Log10
Days
C
Control Group
EHD2K KO Group
Fold Change in Photon Flux (p/s) in Log10
Days
*
D
Control
EHD2 KO
Number of tumor nodules
**
WT
EHD2 KO
E
H&E
EHD2
CK18
IgG
Control
EHD2 KO
M

Fig. 5

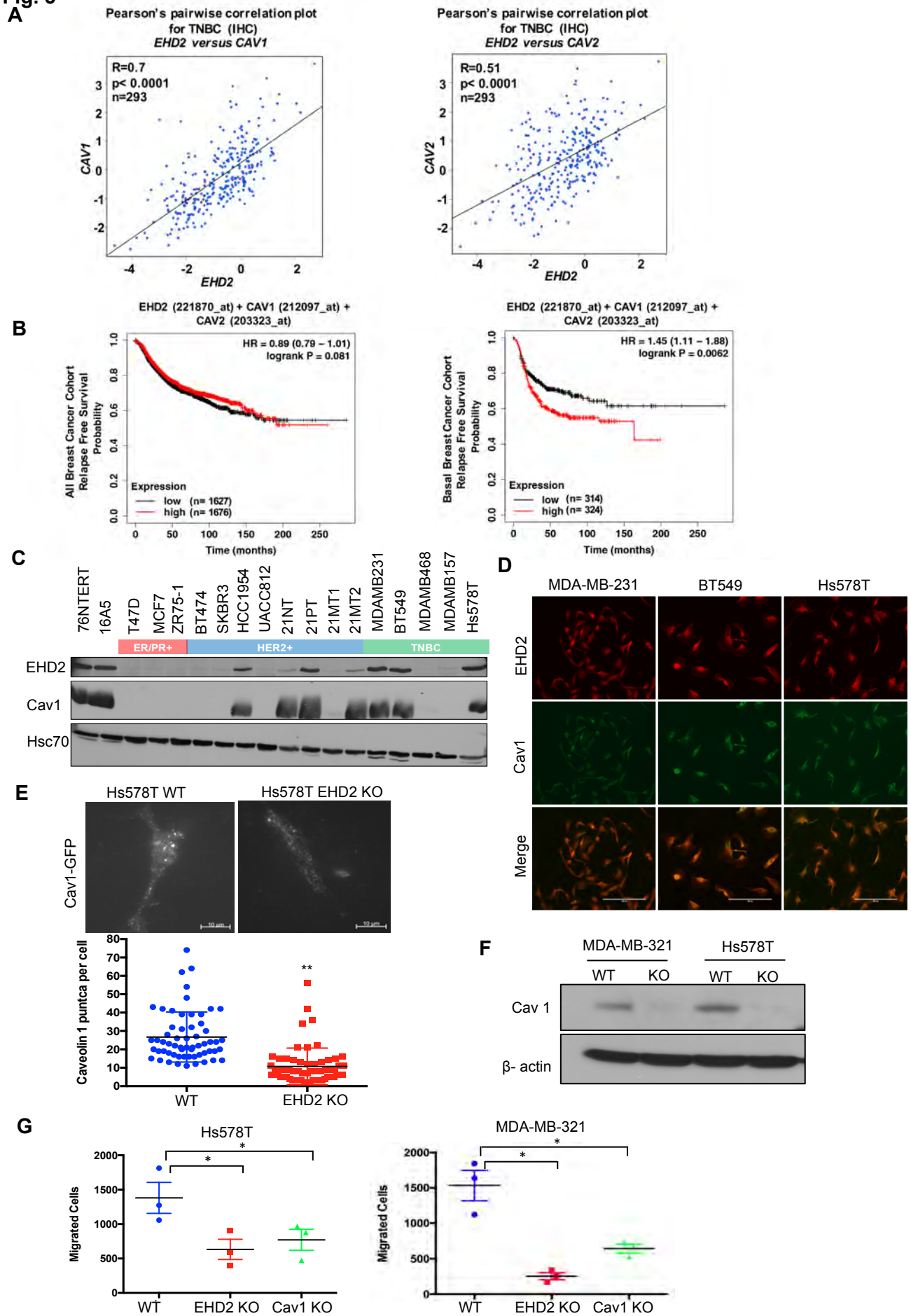
A
Pearson's pairwise correlation plot for TNBC (IHC)
EHD2 versus CAV1
R=0.7
p< 0.0001
n=293
CAV1
EHD2
Pearson's pairwise correlation plot for TNBC (IHC)
EHD2 versus CAV2
R=0.51
p< 0.0001
n=293
CAV2
EHD2
B
EHD2 (221870_at) + CAV1 (212097_at) + CAV2 (203323_at)
All Breast Cancer Cohort Relapse Free Survival Probability
HR = 0.89 (0.79 – 1.01)
logrank P = 0.081
Expression
low (n= 1627)
high (n= 1676)
Time (months)
EHD2 (221870_at) + CAV1 (212097_at) + CAV2 (203323_at)
Basal Breast Cancer Cohort Relapse Free Survival Probability
HR = 1.45 (1.11 – 1.88)
logrank P = 0.0062
Expression
low (n= 314)
high (n= 324)
Time (months)
C
76NTERT
16A5
T47D
MCF7
ZR75-1
BT474
SKBR3
HCC1954
UACC812
21NT
21PT
21MT1
21MT2
MDAMB231
BT549
MDAMB468
MDAMB157
Hs578T
ER/PR+
HER2+
TNBC
EHD2
Cav1
Hsc70
D
MDA-MB-231
BT549
Hs578T
EHD2
Cav1
Merge
E
Hs578T WT
Hs578T EHD2 KO
Cav1-GFP
Caveolin 1 puntca per cell
**
WT
EHD2 KO
F
MDA-MB-321
Hs578T
WT
KO
WT
KO
Cav 1
β- actin
G
Hs578T
Migrated Cells
*
*
WT
EHD2 KO
Cav1 KO
MDA-MB-321
Migrated Cells
*
*
WT
EHD2 KO
Cav1 KO

Fig.6

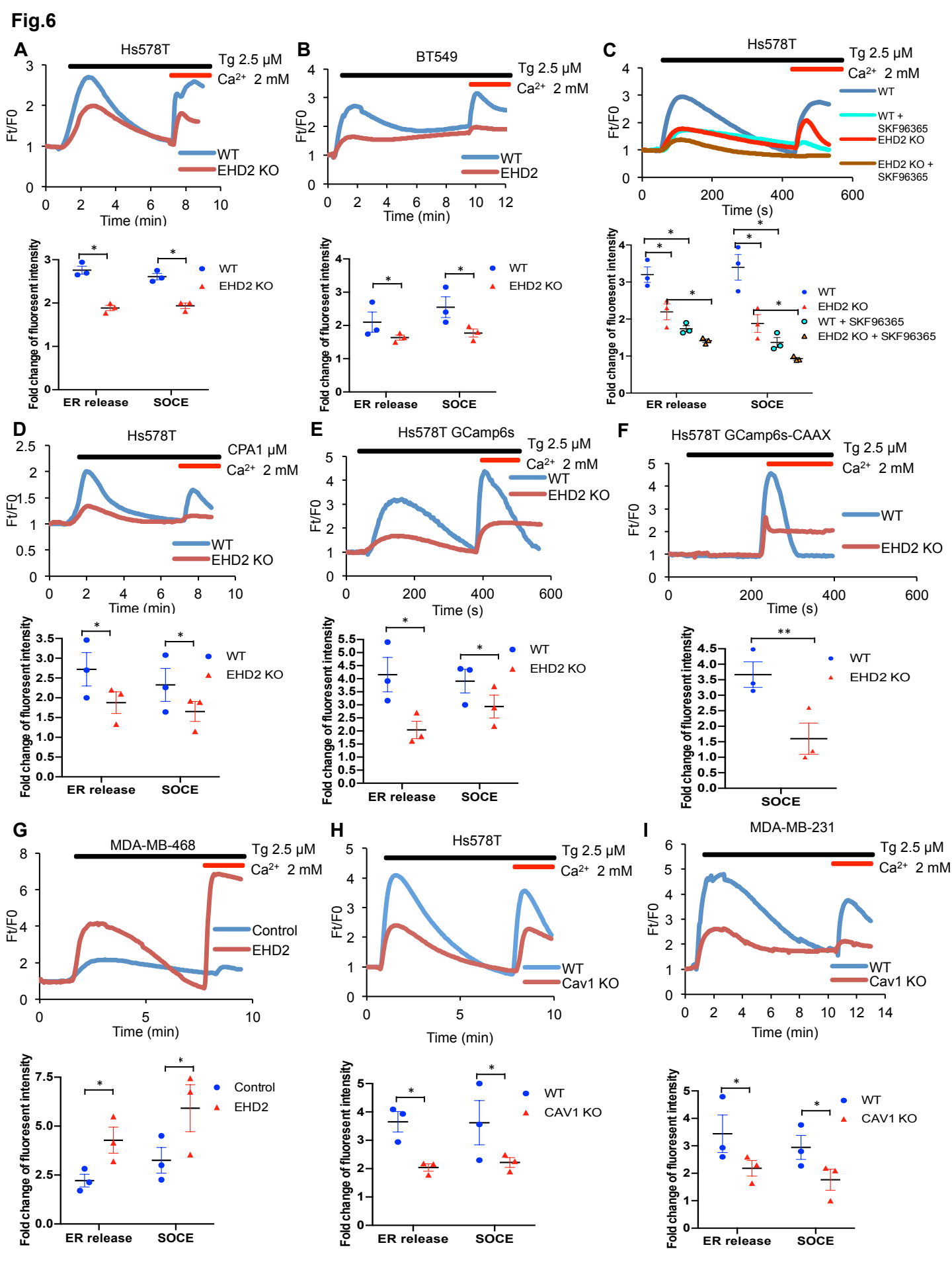
A
Hs578T
Tg 2.5 μM
Ca2+ 2 mM
WT
EHD2 KO
Ft/F0
Time (min)
B
BT549
Tg 2.5 μM
Ca2+ 2 mM
WT
EHD2
Ft/F0
Time (min)
C
Hs578T
Tg 2.5 μM
Ca2+ 2 mM
WT
WT + SKF96365
EHD2 KO
EHD2 KO + SKF96365
Ft/F0
Time (s)
Fold change of fluoresent intensity
ER release
SOCE
WT
EHD2 KO
WT + SKF96365
EHD2 KO + SKF96365
D
Hs578T
CPA1 μM
Ca2+ 2 mM
WT
EHD2 KO
Ft/F0
Time (min)
E
Hs578T GCamp6s
Tg 2.5 μM
Ca2+ 2 mM
WT
EHD2 KO
Ft/F0
Time (s)
F
Hs578T GCamp6s-CAAX
Tg 2.5 μM
Ca2+ 2 mM
WT
EHD2 KO
Ft/F0
Time (s)
G
MDA-MB-468
Tg 2.5 μM
Ca2+ 2 mM
Control
EHD2
Ft/F0
Time (min)
H
Hs578T
Tg 2.5 μM
Ca2+ 2 mM
WT
Cav1 KO
Ft/F0
Time (min)
I
MDA-MB-231
Tg 2.5 μM
Ca2+ 2 mM
WT
Cav1 KO
Ft/F0
Time (min)
CAV1 KO

Fig. 7

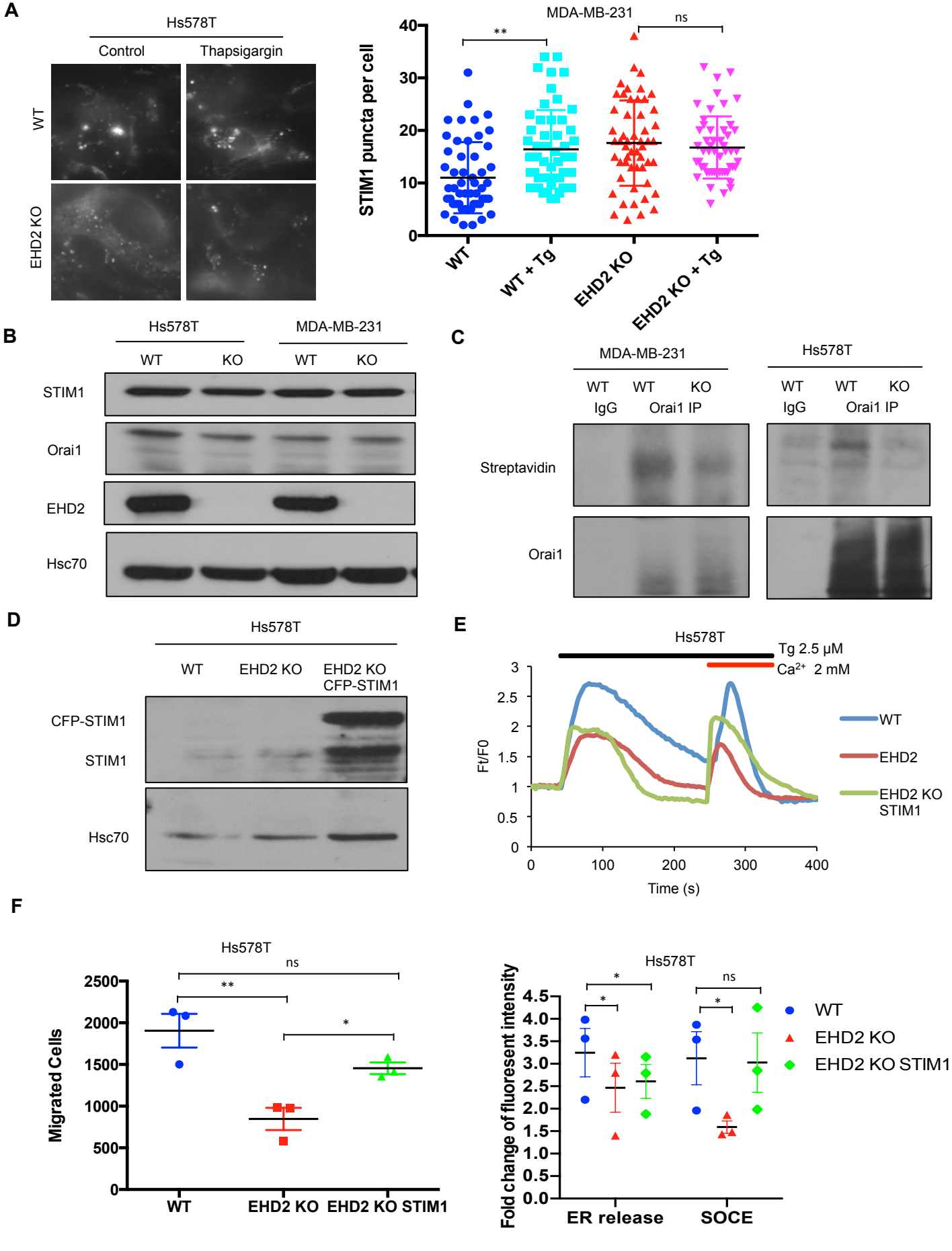
A
Hs578T
Control
Thapsigargin
WT
EHD2 KO
MDA-MB-231
STIM1 puncta per cell
**
ns
WT
WT + Tg
EHD2 KO
EHD2 KO + Tg
B
Hs578T
MDA-MB-231
WT
KO
WT
KO
STIM1
Orai1
EHD2
Hsc70
C
MDA-MB-231
Hs578T
WT
IgG
WT
Orai1 IP
KO
WT
IgG
WT
Orai1 IP
KO
Streptavidin
Orai1
D
Hs578T
WT
EHD2 KO
EHD2 KO CFP-STIM1
CFP-STIM1
STIM1
Hsc70
E
Hs578T
Tg 2.5 μM
Ca2+ 2 mM
Ft/F0
Time (s)
WT
EHD2
EHD2 KO STIM1
F
Hs578T
Migrated Cells
ns
**
*
WT
EHD2 KO
EHD2 KO STIM1
Hs578T
Fold change of fluoresent intensity
*
*
ns
*
WT
EHD2 KO
EHD2 KO STIM1
ER release
SOCE

Fig. 8

A

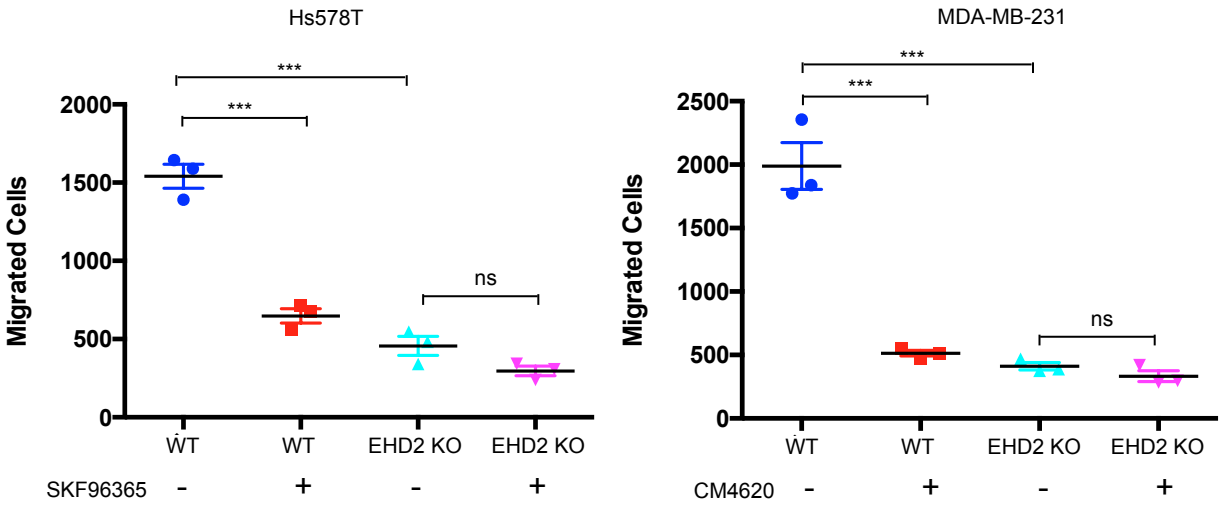
Hs578T
MDA-MB-231
Migrated Cells
***
***
ns
2000
1500
1000
500
0
2500
WT
WT
EHD2 KO
EHD2 KO
SKF96365 - + - +
CM4620 - + - +

B

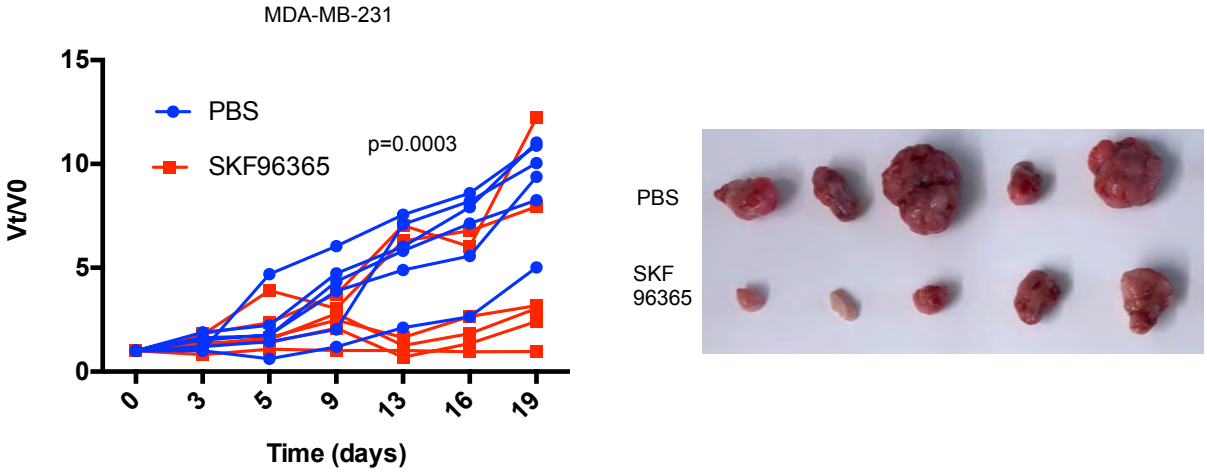
MDA-MB-231
PBS
SKF96365
p=0.0003
Vt/V0
15
10
5
0
0
3
5
9
13
16
19
Time (days)
PBS
SKF
96365